UNIVERSITY OF SÃO PAULO
SÃO CARLOS SCHOOL OF ENGINEERING

Marvin Castro Grossi

Infinite nanocylinders as capacitive and inductive nanoelements in metatronics

São Carlos

2019

Marvin Castro Grossi

Infinite nanocylinders as capacitive and inductive nanoelements in metatronics

Monograph presented to the course of Electrical Engineering with emphasis in Electronics, of the São Carlos School of Engineering of the University of São Paulo, as a prerequisite to obtain the title of Electrical Engineer.

Supervisor: Prof. Dr. Leonardo André Ambrosio

São Carlos

2019

Catalog card prepared by Patron Service at "Prof. Dr. Sergio Rodrigues Fontes" Library at EESC/USP

Grossi, Marvin Castro
G878i Infinite nanocylinders as capacitive and inductive nanoelements in metatronics / Marvin Castro Grossi ; Monograph directed by Leonardo André Ambrosio. -- São Carlos, 2019.

Monograph (Undergraduate Thesis)Undergraduate Program in Electrical Engineering with emphasis in electronics -- São Carlos School of Engineering, at University of São Paulo, 2019.

1. Optical circuit. 2. Nanocylinder. 3. Nanoinductor. 4. Nanocapacitor. 5. Metatronics. 6. Generalized Lorenz Mie theory. 7. Plasmonics. 8. Metamaterial. I. Title.

Elena Luzia Palloni Gonçalves – CRB 8/4464

FOLHA DE APROVAÇÃO

Nome: Marvin Castro Grossi

Título: "Infinite nanocylinders as capacitive and inductive nanoelements in metatronics"

Trabalho de Conclusão de Curso defendido e aprovado em 11 / 06 / 2019,

com NOTA 7,0 (SETE , ZERO), pela Comissão Julgadora:

Prof. Dr. Leonardo André Ambrosio - Orientador - SEL/EESC/USP

Prof. Dr. Emiliano Rezende Martins - SEL/EESC/USP

Prof. Dr. João Paulo Pereira do Carmo - SEL/EESC/USP

Coordenador da CoC-Engenharia Elétrica - EESC/USP:
Prof. Associado Rogério Andrade Flauzino

ACKNOWLEDGEMENTS

I am forever grateful to my family, Marília, Marcos and Marcelo, for the endless love, support and granting the opportunities I had.

I would like to thank my girlfriend Isabella for always being there for me, my friend Jhonatan for the partnership on countless projects, Pedro Theodoro, Cascardo and Henrique for the "ISSAs" and to all my friends around the world.

Moreover, I would like to express my sincere gratitude to Professor Leonardo Ambrosio for the opportunities, support and confidence throughout the past four years.

ABSTRACT

GROSSI, M. C. **Infinite nanocylinders as capacitive and inductive nanoelements in metatronics**. 2019. 54p. Monograph (course completion project) - São Carlos School of Engineering, University of São Paulo, São Carlos, 2019.

Optical circuits have the potential to shift the way data processing is done, bringing a new range of applications. Taking as a starting point complete and to be published studies, the analytic equations for the incident, scattered and internal nanoimpedances associated with the scattering of a plane-wave by an infinite cylinder are successfully deduced. It is done for the case of a wave with arbitrary orientation and a dielectric or plasmonic nanocylinder. The expressions exhibit a dependence on the incidence angle, differently from the case of a nanosphere. The cases for normal and parallel incidence are closely analyzed, exploring the capacitor or inductor behavior depending on the cylinder's material. Latter, results are evaluated for distinct incident angles and array of relative permitivitty, displaying accurately the behavior of the functions. Finally, in order to have visual insights, a visualization of the incident and scattered electric fields is done, using Mathematica software. It is implemented applying explicitly the plane-wave expansion.

Keywords: Optical Circuit. Metatronics. Nano-cylinder. Nano-inductor. Nano-capacitor. Field Expansion. Plasmonics. Metamaterial. Generalized Lorenz Mie Theory. Simulation.

RESUMO

GROSSI, M. C. **Nanocilindros infinitos como nanoelementos capacitivos e indutivos em metatrônica**. 2019. 54p. Monografia (Trabalho de Conclusão de Curso) - Escola de Engenharia de São Carlos, Universidade de São Paulo, São Carlos, 2019.

Circuitos opticos têm o potencial de mudar a maneira como processamento de dados é feito, trazendo novas formas de aplicações. Tomando como ponto de partida estudos completos e a serem publicados, é apresentada a dedução de equações analíticas para nano-impedâncias incidentes, espalhadas e internas, associadas com o espalhamento de um onda plana por um cilindro infinito. Isto foi feito para o caso de um onda de orientação arbitraria e com o nano cilindro dielétrico ou plasmônico. As expressões exibem dependência ao ângulo de incidência, diferentemente do caso de uma nano esfera. Os casos para incidência normal e paralela são analizados de perto, explorando o comportamento de capacitor ou indutor dependendo do material do cilindro. Então, resultados numéricos são avaliados para distintos ângulos de incidência e um segmento de valores de permissividade relativa, mostrando com precisão o comportamento das funções. Finalmente, para obter uma percepção visual, uma simulação dos campos incidentes e espalhados foi feita, utilizando o software Mathematica. Foi implementado aplicando explicitamente as expansões de onda plana.

Palavras-chave: Circuito óptico. Metatrônica. Nano cilindro. Nano indutor. Nano capacitor. Expansão de campos. Material plasmônico. Metamaterial. Teoria de Lorenz Mie generalizada. Simulação.

LIST OF FIGURES

LIST OF ABBREVIATIONS AND ACRONYMS

GLMT	Generalized Lorenz-Mie Theory
EM	Electromagnetic
SMEs	Special Maxwell Equations
TM	Transverse Magnetic mode
TE	Transverse Electric mode

LIST OF SYMBOLS

Z	Impedance	D	Displacement field
i	Imaginary unit	I	Displacement current
ε	Permittivity	N	Displacement current density
μ	Permeability	V	Electric potential
ρ	Electric charge density	$\langle V \rangle$	Average potential difference
ω	Angular frequency	t	Time variable
M	Relative refractive index	U	Bromwich scalar potential
x	Size parameter	$J_m(.)$	Bessel function of the first kind
λ	Wavelength	$Y_m(.)$	Bessel function of the second kind
k	Wave number	$H_m(.)$	Hankel function
ξ	Incident angle	F_m	Mie scattering coefficient
δ	cosξ	S_m	Mie scattering coefficient
a	Diameter of the cylinder	C_m	Mie scattering coefficient
l	Length of the cylinder	L	Inductance
E	Electric field	C	Capacitance
H	Magnetic field		

CONTENTS

1 INTRODUCTION

1.1 Contextualization and Motivation

Since Alessandro Volta invented the electrical battery in 1799, electrical circuits started being developed and have been facing a dramatic improvement. One important concept for this, is the circuit modularization in passive and active elements, in which each one is described by a specific function. Separated parts allow simplification of the modeling of each element, thus establishing an easier path for the improvement. These elements can be lumped to create complex systems with different purposes.

It is important to notice that this "lumped" element modeling is only applicable if the physical size of the circuit is much smaller than its operating wavelength (GERSHENFELD, 2000). All the elements and circuits analyzed in this work follow this rule.

The aforementioned notion has paved the way for the miniaturization of circuits, which is a very important topic to the development of new technologies. The size of the circuit elements shrunk with time and have successfully been used in the radio frequency domain (3 KHz - 300 GHz or 1 mm - 100 Km wavelength) and microwave domain (300 MHz - 300 GHz or 1 mm - 1 m wavelength).

Therefore, the logical next step is to keep downsizing elements and consequently whole circuits to operate in the infrared (300 GHz - 405 THz or 1 mm - 740 nm wavelength) domain and visible spectrum (405 THz - 790 THz or 740 nm - 380 nm wavelength). This could improve information processing, data transfer and storage capacity on embedded tiny equipment. And this could be used for enhancing medicine techniques, communications and others. There are methods and technology available today that make it possible to craft structures in such a small scale. However, one cannot achieve this goal by only downsizing the elements. There are many challenges to the task that emerge and that must be adequately addressed.

One of such challenges is the interaction between materials and the electromagnetic waves in the visible spectrum. At this scale, the most used theories do not apply satisfactorily, and unforeseen couplings between light and matter occur.

There are some noble metals, metal-like materials (WEST et al., 2010) and metamaterials - "artificial materials with unusual electromagnetic properties that are not found in naturally occurring materials" (KSHETRIMAYUM, 2005) - that exhibit negative real permittivity. They are called plasmonic materials. The free electrons in the surface of these materials - in the boundary with a dielectric medium - can sustain collective charge density oscillations (plasmons) that can interact with light and produce propagating electromagnetic waves (surface plasmon polaritons) (CAI; SHALAEV; PAUL, 2010). This allows optical signals to be propagated in an even smaller scale, which can then be used in the miniaturization process.

The concept behind electrical circuits consists of a flow of a quantity (the electrical current as the flow of electrons) related to the potential of another quantity (the electric potential) going through elements with specific functions (the resistors, inductors, capacitors, etc.) (ENGHETA, 2007). For optical circuits, the flow cannot be an electrical current. For that purpose, one must have recourse to another term that comes from the addition made by Maxwell to the Ampère's circuital law: the displacement current

density $\partial \mathbf{D}/\partial t$ (being $\mathbf{D}$ the displacement field) (ENGHETA, 2007).

The notion of nanoelectronics, usually called "metatronics[1]", is in its early stages of development. Some attempts have already been made on designing nanodevices. Nader Engheta and his group introduced the concept of nanoinductors and nanocapacitors using nanospheres (ENGHETA; SALANDRINO; ALÙ, 2005). Since then, many other works have been presented regarding different types of optical nanocircuits (ALÙ; ENGHETA, 2007; SALANDRINO; ALÙ; ENGHETA, 2007; ALÙ; SALANDRINO; ENGHETA, 2007; SILVEIRINHA et al., 2008; ALÙ; ENGHETA, 2009). Recently, researchers designed a metastructure capable of integrating an arbitrary wave as an input function, generating a complex valued electromagnetic field as output (ESTAKHRI; EDWARDS; ENGHETA, 2019).

However, there are still many aspects which can be improved and a lot of room for theoretical as well as applied researches. It is a challenging and fascinating field that demands intellectual capital investment and state-of-the-art techniques. Also, it can lead to important advancements in biological circuits, nano-optics, optical information storage, biophotonics, molecular signaling and so on (ENGHETA; SALANDRINO; ALÙ, 2005). The field is booming with new concepts and designs that are contributing to, one day, having faster complex data processing with light in a nanoscale.

This study approaches the theme by considering the design of a nanoparticle that can act as an inductor or a capacitor depending on the material properties and the plane-wave's incident angle. This is possible defining the geometry of the particle as a cylinder, since it does not have the symmetrical properties the sphere has (which is found in most designs).

1.2 Objectives

This study aims at mathematically modeling elements for optical circuits (for the case of a plane wave) with inductive and capacitive characteristics, using dielectric or plasmonic infinite cylinders in the nanometer scale.

Furthermore, the goal is to analytically determine the expressions and simulate the electric field behavior using the commercial software Mathematica and evaluate the expressions functionality.

Additionally, this study is an extension of one also in metatronics and plasmonics involving different applications. The article is called "Optical Camouflage and Transparency with Metamaterials" (GROSSI; AMBROSIO, 2016). As said, it shares theories and subjects with this study, like plasmonic, metamaterials and Mie Theory for scattering waves. Thus it will expand my knowledge of the field and of electrical engineering in general.

This research is a complementary work to the articles (AMBROSIO; HERNÁNDEZ-FIGUEROA, 2013) and (GROSSI; AMBROSIO, 2019).

Hopefully it will break ground for new technologies and advancements in the field.

[1] Initially, the term was written as "metactronics" (ENGHETA, 2007). Latter it started to be referred to as "metatronics" (ENGHETA, 2011)

1.3 Project Organization

The remainder of this document is organized as follows: Chapter 2 contains the theoretical background, where all the knowledge required to understand this project is presented including specific equation development, i.e., the context regarding the field of study development, the mathematical tools used and the deduction of the necessary equations. Chapter 3 analyzes the equations obtained in a anlytical perspective, using examples, and later a visualization of the fields is done using the commercial software Mathematica. Also, the results are discussed. Finally, in Chapter 4, the conclusions are presented.

2 THEORETICAL BACKGROUND AND DEVELOPMENT

2.1 Initial Considerations

Optical circuits have the same underlying physical principles of electric circuits: electromagnetic theory or, equivalently, Maxwell's equations. Thus, in order to understand the former, it is important to fully comprehend the latter.

Since it is a complex topic, a parallel will be drawn between electrical and optical circuit elements to clarify its functionality and define its desired behavior. However, it is important to keep in mind that some variables might not be the same, as previously said in Chapter 1, for example, in the optical circuit the displacement current density will play the role that the electrical current plays in electrical circuits.

Commonly, the electric circuit fundamentals and equations are thought as a freestanding set of rules. Nevertheless, it all comes from deductions starting from Maxwell's equations and specific conditions.

One of these conditions is that the frequency must be below a given limit so that the total physical size of the circuit is much smaller than the electromagnetic wavelength (GERSHENFELD, 2000). If the size is comparable to the wavelength, the electrical circuit laws do not work and it is necessary to model the problem as transmission lines.

In this study, despite the use of infinite cylinders, we can consider that the nanoscale circuit is much smaller than the wavelength of the impinging wave. Thus, we can draw a parallel between the functionality of the elements of both circuits.

2.2 Impedance

The electrical impedance of a circuit element is quantitatively represented by the ratio of the complex representation of a sinusoidal voltage between its terminals divided by the complex representation of the current flowing through it (CALLEGARO, 2016).

These circuit elements can be labeled as resistors, inductors and capacitors depending on their resistive (real part) and reactive (imaginary part) impedances. There is a general form to depict them. In this work, Cartesian and polar forms will be used to express complex numbers. Resistors can me be expressed as $Z_R = R$, where R is the real part. The inductors are represented as

$$Z_L = i.\omega.L, \tag{2.1}$$

where i is the imaginary unit, ω is the frequency and L is the number or expression for the inductance. Finally, for the capacitors one has

$$Z_C = \frac{1}{i.\omega.C} = -\frac{i}{\omega.C}, \tag{2.2}$$

where C is the number or expression for the capacitance.

One may notice that when the imaginary part of a given impedance assumes negative values, it is classified as a capacitor. Also, when it assumes a positive value, it is considered an inductor. This notion

can be extended to the case of the nanoelements that will be analyzed in the next sections, i.e. negative values of nanoimpedances should be interpreted as nanocapacitors and positive ones as nanoinductors.

This section will be useful for an equation comparison in sections 2.5 and 2.6 of this present chapter.

2.3 The Spherical Case

Since the majority of seminal studies done in the field are for the case of a spherical particle, an overview of it will be briefly given. Then the case for an infinite cylinder will be analyzed.

In 1908, Gustav Mie published a paper that would become the basic building block for a series of studies in electromagnetic wave scattering. The paper describes the interaction between a sphere and a electromagnetic plane wave, using the framework of Maxwell's electromagnetism. Prior to that, applying the same method of separation of variables, Lorenz published an equivalent paper, but relying on the mechanical theory of *aether*. Thus, the theory is referred to as Lorenz-Mie Theory (GOUESBET, 2009).

The physical phenomenon is simple. An incident radiation (light) creates oscillations on the electrons of the particle (sphere in this case). The effect is a secondary radiation known as scattering. Also, a part of the incident radiation is absorbed. These radiations depends on the material and geometrical characteristics of the scatterer.

To mathematically model this problem, the starting point is Maxwell's equations. They are used to deduce the wave equation, that in this case is a plane wave. The problem is reduced to solving only the scalar equation, called the generating function, that benefits from using a more suitable coordinate system (the spherical here). It is in a form of a partial differential equation (PDE) function, that can be transformed to three ordinary differential equation (ODE), using separable coordinates. The solutions must be linearly independent and single-valued. Every solution (incident, scattered and internal fields) can be expanded in the form of infinite series of spherical harmonics. Later, applying the boundary conditions, the Mie coefficients[1] from the solutions can be determined.

In order to evaluate this infinite series, some of the theories were conceived to wisely truncate it without losing precision. The most used one is the dipolar approximation (also known as Rayleigh approximation). In this case, the electric dipolar Mie scattering coefficients are considered, and the magnetic ones are disconsidered, since the relative permeability is considered to be 1, thus only the electric coefficients significantly contributes in the overall phenomenon. For cases where the particle has magnetic properties, those coefficients should be considered. Nevertheless, this approximation is only applicable if:

1. $|M|x << 1$, with M being the relative refractive index of the particle and x the size parameter ($x = 2\pi a/\lambda$);

2. $d << \lambda$, being λ the wavelength of the incident wave and d the dimension of the scatterer.

The problem for a sphere benefits from the geometric symmetry and the final expressions do not depend on the wave's incident angle.

[1] The Mie scattering coefficients are the expansion coefficients of the the scattered field for the Mie solution

2.4 Mathematical Modeling for the Infinite Cylinder Case

In this section, a similar procedure to the one just presented will be developed for the cylinder case.

First, one cannot use the dipolar approximation. Since the particle in analysis is an infinite cylinder, the second condition of the preceeding section is not met. Many other studies were made for more generic cases regarding the interaction of different shaped beams with several other particle shapes, also using the method of separation of variables. Those are labeled as Generalized Lorenz-Mie Theory (GLMT) (GOUESBET, 2009).

In order to mathematically treat the problem, it is necessary to use an equivalent version of the expansion of electromagnetic field components in spherical harmonic functions - found in (BOHREN; HUFFMAN, 1998) - for simple and lossless dielectric and plasmonic cylinders. The EM fields found by this dipole approximation (for the cylinders case) should use at least two cylindrical Mie scattering coefficients, that is, both the dipolar electric and magnetic terms contributes.

It is important to notice that the term "infinite cylinder" should be interpreted as cylinder with its longitudinal dimension z several times longer than its diameter. A fair approximation of this would be $z > 20a$, being a the diameter (BOHREN; HUFFMAN, 1998).

Since the problem is not symetrical as the spherical case is, the nanoimpedance may be a function of the spatial position of the particle, of the direction of propagation of the impinging wave and its polarization.

The goal of this section is to find, with the aid of the GLMT, the explicit closed-form solutions for the average potential difference, displacement currents, internal and fringing nanoimpedances associated with the scattering of a plane wave by an infinite cylinder.

Consider a isotropic, homogeneous, lossless and non-magnetic cylindrical particle with radius a. It is spatially oriented with its axis on the z-axis. The case for a parallel impinging electromagnetic plane wave will be addressed first. It propagates along the x-z plane according to the function $\hat{\mathbf{e}}_i = -sin\xi\hat{\mathbf{e}}_x - cos\xi\hat{\mathbf{e}}_z$ having a time harmonic factor $exp(i\omega t)$. The latter will be omitted in order to make the equations less cumbersome. Thus, the incident electric field can be described, in cylindrical coordinates (ρ, ϕ, z), as

$$\mathbf{E}_i^{//} = E_0(\sin\xi\hat{\mathbf{e}}_z - \cos\xi\hat{\mathbf{e}}_x) \times \exp[ik(\rho\sin\xi\cos\phi + z\cos\xi)], \tag{2.3}$$

in which E_0 is the field strength, k the wave number, ξ the incident angle relative to the axis of the cylinder.

For the case of a perpendicular polarization, where the electric field vibrates along the y-direction, the equation is expressed as

$$\mathbf{E}_i^{\perp} = E_0\hat{\mathbf{e}}_y \exp[ik(\rho\sin\xi\cos\phi + z\cos\xi)] \tag{2.4}$$

In order to find the equation for the impedance, it is necessary to describe the current and average potential difference. As it was said before, in this case the displacement current will be used. So its continuity along $\rho = a$ will be analyzed. The average potential difference will be calculated between the surface of two hemispheres, defined by $(\rho = a, -\pi/2 < \phi < \pi/2, z)$ and $(\rho = a, \pi/2 < \phi < 3\pi/2, z)$.

From this, one can conclude that only the radial component E_ρ of the electric field matters here, which will be the basis for the deduction of closed-form solutions.

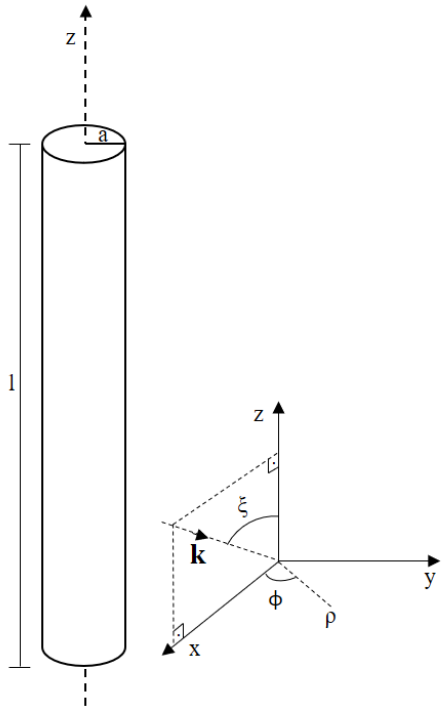

Figure 1: Illustrative image of the cylinder orientation and electric field

2.4.1 The Bromwich Method

Before beginning, it should be mentioned that there are a couple of ways to solve the Mie scattering equations among researchers. The most popular one is the use of Hertz-Debye potentials, which are written in vectorial form using vector wave functions (GOUESBET; GRÉHAN,). Although it is the most concise way, historically the studies regarding the Lorenz Mie Theory uses the Bromwich method, that is based on scalar potentials. Since the methods are equivalent and the articles (GROSSI; AMBROSIO, 2019) and (AMBROSIO; HERNÁNDEZ-FIGUEROA, 2013) use the Bromwich method, the scalar option has been chosen.

The following deductions (until subsection 2.4.3 "Wave Expansion") have also been detailed in (GOUESBET; GRÉHAN, 1994) and (GOUESBET, 1997). The building block is the GLMT applied to cylindrical scatterers. Also, it is important to emphasize that this work will only use the fundamental equations necessary to the development of this study and will not detail the mathematical formalism.

When the media is linear, local, isotropic and homogeneous (which is the case), the Maxwell equations can be simplified to the special Maxwell equations (SMEs). A known method to solve these equations, as mentioned before, is the Bromwich method. To use it, one needs to use an orthogonal curvilinear coordinate system.

For any point P in the cylindrical coordinate system $(z, \rho, \phi) = (x_1, x_2, x_3)$. Applying Pythagoras' theorem, one has (GOUESBET; GRÉHAN, 1994):

$$ds^2 = (e_1)^2 dz^2 + (e_2)^2 d\rho^2 + (e_3)^2 d\phi^2 \tag{2.5}$$

, being ds an infinitesimal distance. Thus

$$e_1 = e_2 = 1, e_3 = \rho \tag{2.6}$$

Then,

$$\begin{aligned} e_1 &= 1, \\ \frac{\partial}{\partial x_1}\left(\frac{e_2}{e_3}\right) = \frac{\partial}{\partial z}\left(\frac{1}{\rho}\right) &= 0 \end{aligned} \tag{2.7}$$

Any solution to the SMEs in this method are a summation of two linearly independent solutions, the Transverse Magnetic wave (TM) and the Transverse Electric wave (TE). The TE mode is characterized by having no electric field in the direction of propagation of the wave, i.e., the electric field is always perpendicular to **k**. Additionally, in the TM mode, the magnetic field is always perpendicular to the direction of propagation.

Applying Gauss, Faraday and Ampère laws with components e_1, e_2 and e_3 in Maxwell equations, and after some algebra, one can derive the following equations for the two pairs of special solutions ($\mathbf{E}_{TM}, \mathbf{H}_{TM}$) and ($\mathbf{E}_{TE}, \mathbf{H}_{TE}$):

$$E_{z,TM} = \frac{\partial^2 U_{TM}}{(\partial z)^2} + k^2 U_{TM} \tag{2.8}$$

$$E_{\rho,TM} = \frac{\partial^2 U_{TM}}{\partial z \partial \rho} \tag{2.9}$$

$$E_{\phi,TM} = \frac{1}{\rho}\frac{\partial^2 U_{TM}}{\partial z \partial \phi} \tag{2.10}$$

$$H_{z,TM} = 0 \tag{2.11}$$

$$H_{\rho,TM} = \frac{i\omega\varepsilon}{\rho}\frac{\partial U_{TM}}{\partial \phi} \tag{2.12}$$

$$H_{\phi,TM} = -i\omega\varepsilon\frac{\partial U_{TM}}{\partial \rho} \tag{2.13}$$

$$E_{z,TE} = 0 \tag{2.14}$$

$$E_{\rho,TE} = -\frac{i\omega\mu}{\rho}\frac{\partial U_{TE}}{\partial \phi} \tag{2.15}$$

$$E_{\phi,TE} = i\omega\mu\frac{\partial U_{TE}}{\partial \rho} \tag{2.16}$$

$$H_{z,TE} = \frac{\partial^2 U_{TE}}{(\partial z)^2} + k^2 U_{TE} \tag{2.17}$$

$$H_{\rho,TE} = \frac{\partial^2 U_{TE}}{\partial z \partial \rho} \tag{2.18}$$

$$H_{\phi,TE} = \frac{1}{\rho}\frac{\partial^2 U_{TE}}{\partial z \partial \phi}, \tag{2.19}$$

being ε the permittivity and μ the permeability.

The solutions may be found solving a partial differential equation (as consequence of Amperère's law) for Bromwich Scalar Potentials (BSP), which in this case are represented by U_{TM} and U_{TE}. For the cylindrical coordinate system, the equation reads as:

$$\frac{\partial^2 U}{\partial z^2} + k^2 U + \frac{1}{\rho}\frac{\partial}{\partial \rho}\rho\frac{\partial U}{\partial \rho} + \frac{1}{\rho^2}\frac{\partial^2 U}{\partial \phi^2} = 0, \tag{2.20}$$

being U valid for U_{TM} and U_{TE}.

With the values for U found for the equation 2.20, one can find the TM and TE components for the electric and magnetic fields.

2.4.2 Separation of Variables

As previously said, GLMT uses the separability of variables to find the closed-form solutions. There exists only eleven separable coordinate systems (GOUESBET; GRÉHAN, 1994) and, not coincidentally, one of them is the cylindrical. So one can find separate solutions for each component.

The solutions to equation 2.20 are found using the separability according to

$$U(z, \rho, \phi) = Z(z)R(\rho)\Phi(\phi) \tag{2.21}$$

Replacing the equation 2.21 in the BSP equation 2.20, one get that the functions $Z(z), R(\rho), \Phi(\phi)$ satisfy:

$$\frac{d^2\phi}{d\phi^2} + b\phi = 0 \tag{2.22}$$

$$\frac{d^2 Z}{dz^2} + aZ = 0 \tag{2.23}$$

$$\rho\frac{d}{d\rho}\left(\rho\frac{dR}{d\rho}\right) + (k^2\rho^2 - a\rho^2 - b)R = 0 \tag{2.24}$$

Using the continuity condition to equation 2.22, requiring that the solution of equation 2.23 remain finite and using $R(\rho) = \Re(r)$ in equation 2.24 - details can be found at (GOUESBET; GRÉHAN, 1994) -, one may obtain, according to the separability dogma, that the general BSPs are a linear combination of a generating function described as:

$$G(z, \rho, \phi) = \begin{pmatrix} J_m(r) \\ Y_m(r) \\ H_m^{(1)}(r) \\ H_m^{(2)}(r) \end{pmatrix} \exp(im\phi)\exp(ik\delta z), \tag{2.25}$$

being $m\epsilon Z$, $J_m(r)$ the first kind of Bessel function, $Y_m(r)$ the second kind of Bessel function, $H_m^{(1)}(r)$ a Hankel function denoted by $H_m^{(1)}(r) = J_m(r) + iY_m(r)$ and $H_m^{(2)}(r)$ another Hankel function denoted by $H_m^{(2)}(r) = J_m(r) - iY_m(r)$. Also, $\delta = cos\xi$ and $r = k\rho\sqrt{1-\delta^2}$.

2.4.3 Wave Expansion

2.4.3.1 Incident Wave Expansion

From the Bessel and Hankel functions introduced in the last section, only $J_m(r)$ does not diverge at $r = 0$. Thus, it must be chosen in the function to generate the BSPs that read as

$$U_{TM}^i = \frac{E_0}{k^2} \sum_{m=-\infty}^{+\infty} (-i)^m F_{m,TM} J_m(r) \exp(im\phi) \exp(ik\delta z) \tag{2.26}$$

$$U_{TE}^i = \frac{H_0}{k^2} \sum_{m=-\infty}^{+\infty} (-i)^m F_{m,TE} J_m(r) \exp(im\phi) \exp(ik\delta z), \tag{2.27}$$

in which $F_{m,TM}$ and $F_{m,TE}$ are the beam shape coefficients. They can be determined by using the orthogonality relation - details can be found at (GOUESBET; GRÉHAN, 1994).

$$F_{m,TM} = \frac{\exp(-k\delta z)}{2\pi(1-\delta^2)(-i)^m J_m(r)} \int_0^{2\pi} (E_z^i/E_0) \exp(im\phi) d\phi \tag{2.28}$$

$$F_{m,TE} = \frac{\exp(-k\delta z)}{2\pi(1-\delta^2)(-i)^m J_m(r)} \int_0^{2\pi} (H_z^i/H_0) \exp(im\phi) d\phi \tag{2.29}$$

Using equations 2.26, 2.27 and equations 2.9, 2.12, 2.15 and 2.18 one may derive all incident field components. Since, as previously discussed, the only component that matters to us is the radial one:

$$E_\rho^i = E_0 \sum_{m=-\infty}^{+\infty} (-i)^m \left[i\delta\sqrt{1-\delta^2} F_{m,TM} J'_m(r) + \frac{m}{k\rho} F_{m,TE} J_m(r) \right] \exp(im\phi) \exp(ik\delta z) \tag{2.30}$$

As said previously in section 2.3, the equation can be truncated for the two first components ($m = 0$ and $m = 1$). After some algebraic work, it reads as

$$E_\rho^i = -iE_0\delta \left[J'_0(r) - 2iJ'_1(r) cos\phi \right] exp(ik\delta z) \tag{2.31}$$

2.4.3.2 Scattered Wave Expansion

$H_m^{(2)}(r)$ must be chosen in the generating function 2.25 for the outgoing wave. The BSPs for the scattered wave are

$$U_{TM}^s = -\frac{E_0}{k^2} \sum_{m=-\infty}^{+\infty} (-i)^m S_{m,TM} H_m^{(2)}(r) \exp(im\phi) \exp(ik\delta z) \tag{2.32}$$

$$U_{TE}^s = \frac{H_0}{k^2} \sum_{m=-\infty}^{+\infty} (-i)^m S_{m,TE} H_m^{(2)}(r) \exp(im\phi) \exp(ik\delta z), \tag{2.33}$$

in which $S_{m,TM}$ and $S_{m,TE}$ are the Mie Scattering coefficients. They are found by imposing the continuity of tangential fields over the surface - details can be found at (GOUESBET; GRÉHAN, 1994).

Using equations 2.32, 2.33 and equations 2.9, 2.12, 2.15 and 2.18 one may derive all incident field components. The radial component reads as

$$E_\rho^s = E_0 \sum_{m=-\infty}^{+\infty} (-i)^m \Big[-i\delta(1-\delta^2) S_{m,TM} H_m'^{(2)}(r) + \frac{m}{k\rho} S_{m,TE} H_m^{(2)}(r) \Big] \exp(im\phi) \exp(ik\delta z) \quad (2.34)$$

As said previously in section 2.3, the equation can be truncated for the two first components ($m = 0$ and $m = 1$). After some algebraic work, it reads as

$$\begin{aligned} E_\rho^s = E_0 \Big\{ -i\delta\sqrt{1-\delta^2} S_{0,TM} H_0'^{(2)}(r) - 2i \Big[-i\delta\sqrt{1-\delta^2} S_{1,TM} H_1'^{(2)}(r) + \\ S_{1,TE} H_1'^{(2)}(r)/(k\rho) \Big] \cos\phi \Big\} \exp(ik\delta z) \end{aligned} \quad (2.35)$$

2.4.3.3 Internal Wave Expansion

Here, the J_m should be used in the generating function to avoid divergences at $\rho = 0$. Also, the wave-number k must be replaced for k_c, being $k_c = kM$. Consequently one will have $\varepsilon_c = \varepsilon k_c^2/k^2 = M^2\varepsilon$ and $r_c = k\rho\sqrt{M^2 - \delta^2}$. The BSPs for the internal wave are

$$U_{TM}^c = \frac{E_0}{k^2 M} \sum_{m=-\infty}^{+\infty} (-i)^m C_{m,TM} J_m(r_c) \exp(im\phi) \exp(ik\delta z) \quad (2.36)$$

$$U_{TE}^c = \frac{iH_0}{k^2} \sum_{m=-\infty}^{+\infty} (-i)^m C_{m,TE} J_m(r_c) \exp(im\phi) \exp(ik\delta z), \quad (2.37)$$

in which $C_{m,TM}$ and $C_{m,TE}$ are the Mie Scattering (internal) coefficients. They are found by imposing the continuity of tangential fields over the surface - details can be found at (GOUESBET; GRÉHAN, 1994).

Using equations 2.36, 2.37 and equations 2.9, 2.12, 2.15 and 2.18 one may derive all incident field components. The radial component reads as

$$E_\rho^c = iE_0 \sum_{m=-\infty}^{+\infty} (-i)^m \Big[\frac{\delta}{M} \sqrt{M^2 - \delta^2} C_{m,TM} J_m'(r_c) + \frac{m}{k\rho} C_{m,TE} J_m(r_c) \Big] \exp(im\phi) \exp(ik\delta z) \quad (2.38)$$

As said previously in section 2.3, the equation can be truncated for the two first components ($m = 0$ and $m = 1$). After some algebraic work, it reads as

$$E_\rho^c = -iE_0 \Big\{ \delta\sqrt{M^2 - \delta^2} C_{0,TM} J_0'(r_c)/M - 2i \Big[\delta\sqrt{M^2 - \delta^2} C_{1,TM} J_1'(r_c)/M + C_{1,TE} J_1(r_c)/(k\rho) \Big] \cos\phi \Big\} \exp(ik\delta z) \quad (2.39)$$

2.4.4 Nanoimpedance for Parallel Polarization

The detailed process to deduce the equations in this chapter can also be found at (GROSSI; AMBROSIO, 2019).

The generic equations for the components of the radial electric field (2.30, 2.34 and 2.39), can be simplified . Since the physical dimensions and the electromagnetic properties of the cylinder ($x << 1$ and $|M|x << 1$), the expansion of the field, that sums over m from $-\infty$ to $+\infty$, can be truncated for $m = 0$ and 1. And, as discussed in (BOHREN; HUFFMAN, 1998), the coefficients $S_{m,TM}$ and $S_{m,TE}$ become negligible for $m > 1$ in this regime.

It is known that the electrical potential of a surface in an instant moment in time is given by the integral of the electric field over the surface as follows

$$V_E = -\int\int E_\rho . d\phi . dz \tag{2.40}$$

This is only valid considering a quasistatic approximation, where $\bigtriangledown \times E$ is locally zero[2] (ENGHETA, 2007). The limits for the integral are the length of the cylinder in z and the angles that define the two hemispheres of the cylinder $(-\pi/2 < \phi < \pi/2)$ and $(\pi/2 < \phi < 3\pi/2)$.

Using the equation defined above 2.40 with $E = E^c - E^i$ (E^c from 2.30 and E^i from 2.39), the average potential difference $\langle V \rangle$ between the two planes defined by $(\rho = a, -\pi/2 < \phi < \pi/2, z)$ and $(\rho = a, \pi/2 < \phi < 3\pi/2, z)$ results in

$$Z = \frac{\langle V \rangle}{I} \tag{2.41}$$

$$Z = \frac{V}{i} \tag{2.42}$$

$$\begin{aligned}\langle V \rangle_{//} = -i\delta 2E_0 \Bigg\{ (V_1(0)/D(0)) \int_0^a J_0'(r_c) d\rho - \int_0^a J_0'(r) d\rho - (4i/\pi) \Bigg[(V_1(1)/D(1)) \int_0^a J_1'(r_c) d\rho \\ + (V_2(1)/D(1)) \int_0^a \frac{1}{\rho} J_1(r_c) d\rho - \int_0^a J_1'(r_c) d\rho \Bigg] \Bigg\} \left(\frac{1}{l} \int_{-l/2}^{l/2} \exp(ik\delta z) dz \right)\end{aligned} \tag{2.43}$$

It is known that the displacement current is given by

$$I_D = -\int\int N_D . d\phi . dz, \tag{2.44}$$

being N the displacement current density, given by

$$N_D = \frac{\partial(\varepsilon E)}{\partial t}, \tag{2.45}$$

where ε is the electric permittivity.

The limits for the integral are the same for evaluating V_E.

[2] Rigorous verification of $\bigtriangledown \times E$ being locally zero was not a part of this study, however it will be considered in following works

For the currents, one can use the same approach used in (ENGHETA; SALANDRINO; ALÙ, 2005), but for cylindrical coordinates instead of spherical. Thus, integrating, over the surface, the equation for the continuity of the displacement current (which depends on E^c from 2.30 and E^i from 2.39) one has

$$I^i_{//} = i\omega a E_0(\varepsilon_0 - \varepsilon)(-i\delta)\big[\pi J_0'(r) - 4iJ_1'(r)\big]\left(\int_{-l/2}^{l/2} \exp(ik\delta z)dz\right) \tag{2.46}$$

$$\begin{aligned} I^s_{//} = i\omega a\varepsilon_0 E_0(i\delta)\big\{\pi(L_1(0)/D(0))H_0'(r) - 4i\big[(L_1(1)/D(1))H_1'(r) \\ +V_3(1)H_1(r)\big]\big\}\left(\int_{-l/2}^{l/2} \exp(ik\delta z)dz\right) \end{aligned} \tag{2.47}$$

$$\begin{aligned} I^c_{//} = i\omega a\varepsilon_0 E_0(-i\delta)\big\{\pi(V_1(0)/D(0))J_0'(r_c) - J_0'(r) - 4i\big[(V_1(1)/D(1))J_1'(r_c) \\ +(V_2(1)/aD(1))J_1(r_c) - J_1'(r)\big]\big\}\left(\int_{-l/2}^{l/2} \exp(ik\delta z)dz\right), \end{aligned} \tag{2.48}$$

being $I^i_{//}$, $I^s_{//}$, $I^c_{//}$ the incident, scattered and internal displacement currents respectively. L_1, D, V_1, V_2 and V_3 are coefficients to be determined.

Applying the tangential continuity of the electrical and magnetic fields as boundary conditions given by

$$E^i_z + E^s_z = E^c_z \tag{2.49}$$

$$E^i_\phi + E^s_\phi = E^c_\phi \tag{2.50}$$

$$H^i_z + H^s_z = H^c_z \tag{2.51}$$

$$H^i_\phi + H^s_\phi = H^c_\phi \tag{2.52}$$

One may deduce the expressions for $V_1(m)$, $V_2(m)$, $V_3(m)$, $L_1(m)$ and $D(m)$:

$$V_1(m) = -(ka)^2(1-\delta^2)^{3/2}(M^2-\delta^2) \times \big[(1-\delta^2)^{1/2}A_2(m) - (M^2-\delta^2)^{1/2}A_3(m)\big] \tag{2.53}$$

$$V_2(m) = -am^2(1-M^2)(1-\delta^2)A_{14}(m)A_4(m) \tag{2.54}$$

$$V_3(m) = m^2(M^2-\delta^2)A_{14}(m)A_1(m) \tag{2.55}$$

$$L_1(m) = (ka)^2(1-\delta^2)^{3/2}(M^2-\delta^2)^{3/2}\left[M^2A_{10}(m)+A_{11}(m)\right] + m^2\delta^2(M^2-1)^2A_7(m) \\ -(ka)^2(1-\delta^2)(M^2-\delta^2)\times\left[(M^2-\delta^2)A_8(m)+M^2(1-\delta^2)A_9(m)\right] \tag{2.56}$$

$$D(m) = (ka)^2(1-\delta^2)^{3/2}(M^2-\delta^2)^{3/2}(M^2+1)A_{12}(m) + m^2\delta^2(M^2-1)^2A_{13}(m) \\ -(ka)^2(1-\delta^2)(M^2-\delta^2)\times\left[(M^2-\delta^2)A_6(m)+M^2(1-\delta^2)A_5(m)\right], \tag{2.57}$$

in which

$$A_1 = J_m(r_c)^2$$

$$A_2 = J'_m(r_c)H_m(r)$$

$$A_3 = J_m(r_c)H'_m(r)$$

$$A_4 = J_m(r_c)H_m(r)$$

$$A_5 = [J'_m(r_c)H_m(r)]^2$$

$$A_6 = [J_m(r_c)H'_m(r)]^2$$

$$A_7 = J_m(r)J_m(r_c)^2H_m(r)$$

$$A_8 = J_m(r_c)^2J'_m(r)H'_m(r)$$

$$A_9 = J_m(r)J'_m(r_c)^2H_m(r)$$

$$A_{10} = J_m(r)J_m(r_c)H'_m(r)J'_m(r_c)$$

$$A_{11} = J_m(r_c)J'_m(r)J'_m(r_c)H_m(r)$$

$$A_{12} = J_m(r_c)J'_m(r_c)H_m(r)H'_m(r)$$

$$A_{13} = [J_m(r_c)H_m(r)]^2$$

$$A_{14} = H_m(r)J'_m(r) - H'_m(r)J_m(r)$$

The expressions above are exactly the equation (79)-(92) from (ENGHETA; SALANDRINO; ALÙ, 2005). Also, the Bessel and Hankel functions ($J_m(.)$ and $H_m(.)$) and their derivatives can be expanded in power series:

$$J_0(\varsigma) \approx 1 - \frac{\varsigma^2}{4}$$

$$J_1(\varsigma) \approx \frac{\varsigma}{2} - \frac{\varsigma^3}{16}$$

$$J'_0(\varsigma) \approx -\frac{\varsigma}{2} + \frac{\varsigma^3}{16}$$

$$J'_1(\varsigma) \approx \frac{1}{2} - \frac{3\varsigma^2}{16}$$

$$H_0(\varsigma) \approx 1 - \frac{\varsigma^2}{4} - \frac{2i[0.577216 + log(\varsigma/2)]}{\pi}$$

$$H_1(\varsigma) \approx \frac{2i}{\pi\varsigma} + \frac{\varsigma}{2} - \frac{\varsigma^3}{16}$$

$$H_0'(\varsigma) \approx -\frac{2i}{\pi\varsigma} - \frac{\varsigma}{2} + \frac{\varsigma^3}{16}$$

$$H_1'(\varsigma) \approx -\frac{2i}{\pi\varsigma^2} + \frac{1}{2} - \frac{3\varsigma^2}{16}$$

Equations 2.43, 2.46-2.48 can be simplified by substituting the equations above (the A_m, Bessel and Hankel functions) to find the closed-form solutions for the average potential difference and total displacement currents for parallel polarization are obtained, and read as

$$\langle V \rangle_{//} = \frac{4E_0\delta}{\pi}\left[\frac{(M^2-1)(M^2+1-\delta^2)}{(M^2+1)(M^2-\delta^2)}\right]\left(\frac{1}{l}\int_{-l/2}^{l/2}\exp(ik\delta z)dz\right) \tag{2.58}$$

$$I^i_{//} = 2iE_0\delta\omega\varepsilon_0 a(M^2-1)\left(\int_{-l/2}^{l/2}\exp(ik\delta z)dz\right) \tag{2.59}$$

$$I^s_{//} = -2iE_0\delta\omega\varepsilon_0 a\left(\frac{M^2-1}{M^2+1}\right)\left(\int_{-l/2}^{l/2}\exp(ik\delta z)dz\right) \tag{2.60}$$

$$I^c_{//} = 2iE_0\delta\omega\varepsilon_0 a\left(M^2\frac{M^2-1}{M^2+1}\right)\left(\int_{-l/2}^{l/2}\exp(ik\delta z)dz\right) \tag{2.61}$$

It is known that complex impedance is given by

$$Z = \frac{V}{I} \tag{2.62}$$

Finally, substituting the equations 2.58-2.61 in the equation 2.62 the fringing and internal nanoimpedances for parallel polarization are obtained:

$$Z^c_{//} = -i\frac{2}{l\pi\omega a\varepsilon_0}\frac{1+M^2-\delta^2}{M^2(M^2-\delta^2)} \tag{2.63}$$

$$Z^s_{//} = i\frac{2}{l\pi\omega a\varepsilon_0}\frac{1+M^2-\delta^2}{(M^2-\delta^2)} \tag{2.64}$$

Analyzing the equations above, one may conclude that the fringing and internal nanoimpedances depend on the impinging wave angle of incidence, cylinder dimensions and the relative refractive index of the material.

2.4.5 Nanoimpedance for Perpendicular Polarization

After finding the closed-form solutions for the nanoimpedances for the case of a incident electric field with a parallel vibration, one may also find the results for the perpendicular case following the same steps.

Now, one must consider the wave equation 2.4 and then with the radial components of the electric field (E^i_ρ from 2.30, E^s_ρ from 2.34, E^c_ρ from 2.39), find the average potential difference between the hemispheres given by $(\rho = a, -\pi/2 < \phi < \pi/2, z)$ and $(\rho = a, \pi/2 < \phi < 3\pi/2, z)$:

$$\begin{aligned}\langle V\rangle_\perp = i\delta 2E_0\Bigg\{(V_4(0)/D(0))\int_0^a J_0'(r_c)d\rho - (4i/\pi D(1))\times\Bigg[V_4(1)\int_0^a J_1'(r_c)d\rho \\ +V_5(1)\int_0^a \frac{1}{\rho}J_1(r_c)d\rho + V_6(1)\int_0^a J_1'(r_c)d\rho\Bigg]\Bigg\}\Bigg(\frac{1}{l}\int_{-l/2}^{l/2}\exp(ik\delta z)dz\Bigg)\end{aligned} \tag{2.65}$$

For the currents, one can integrate over the surface the equation for the continuity of the displacement current (which depends on E^c from 2.30 and E^i from 2.39) and find

$$I^i_\perp = i\omega a E_0(\varepsilon_0 - \varepsilon)\left[\frac{4}{k\sqrt{1-\delta^2}}J_1(r)\right]\Bigg(\int_{-l/2}^{l/2}\exp(ik\delta z)dz\Bigg) \tag{2.66}$$

$$\begin{aligned}I^s_\perp = i\omega a\varepsilon_0 E_0(-i\delta)\big\{\pi(L_2(0)/D(0))H_0'(r) + (4/D(1))\big[L_2(1)H_1'(r) \\ +V_7(1)H_1(r)\big]\big\}\Bigg(\int_{-l/2}^{l/2}\exp(ik\delta z)dz\Bigg)\end{aligned} \tag{2.67}$$

$$\begin{aligned}I^c_\perp = i\omega a\varepsilon_0 E_0(i\delta)\big\{\pi(V_4(0)/D(0))J_0'(r_c) + (4/D(1))\times\big[V_4(1)J_1'(r_c) \\ +a^{-1}V_5(1)J_1(r_c)a^{-1}V_6(1)J_1(r)\big]\big\}\Bigg(\int_{-l/2}^{l/2}\exp(ik\delta z)dz\Bigg)\end{aligned} \tag{2.68}$$

Using the same boundary conditions used for the parallel case (equations 2.49 to 2.52), one may deduce the expressions for the coefficients $V_4(m)$, $V_5(m)$, $V_6(m)$, $V_7(m)$ and $L_2(m)$:

$$V_4(m) = i(ka)(m\delta)(M^2-1)(M^2-\delta^2)^{1/2}(1-\delta^2)A_{14}(m)A_4(m) \tag{2.69}$$

$$V_5(m) = \frac{im}{k\delta}(ka)^2(1-\delta^2)^{3/2}(M^2-\delta^2)^{1/2}\big[M^2(1-\delta^2)^{1/2}A_2(m) - (M^2-\delta^2)^{1/2}A_3(m)\big] \tag{2.70}$$

$$\begin{aligned}V_6(m) = \frac{im}{k\delta}(ka)^2(1-\delta^2)^{1/2}(M^2-\delta^2)^{3/2}\Bigg\{(1-\delta^2)^{1/2}(M^2+1)A_{12}(m) - (M^2-\delta^2)^{1/2} \\ \times\big[(M^2-\delta^2)A_6(m) + M^2(1-\delta^2)A_5(m)\big] + m^2\delta\frac{(M^2-1)^2}{(1-\delta^2)^{1/2}}A_{13}(m)\Bigg\}\end{aligned} \tag{2.71}$$

$$V_7(m) = \frac{im}{ka\delta(1-\delta^2)^{1/2}}\Bigg\{ -(ka)^2(1-\delta^2)^{3/2}(M^2-delta^2)^{3/2}\times\Big[M^2A_{11}(m) + A_{10}(m)\Big] - m^2\delta^2(M^2-1)^{1/2}A_7(m) + (ka)^2(1-\delta^2)(M^2-delta^2) + \Big[(M^2-delta^2)A_8(m) + M^2(1-delta^2)A_9(m)\Big]\Bigg\} \tag{2.72}$$

$$L_2(m) = -i(ka)(m\delta)(M^2-delta^2)(1-delta^2)^{1/2}A_{14}(m)A_1(m) \tag{2.73}$$

Using equations 2.69-2.73 and the A_m, Bessel and Hankel functions expanded in power series, one can simplify equations 2.65, 2.66, 2.67 and 2.68 to

$$\langle V\rangle_\perp = \frac{4E_0}{k\pi}\left[\frac{(M^2-1)(2k\delta^2-M^2ka)}{(M^2+1)(M^2-\delta^2)}\right]\left(\frac{1}{l}\int_{-l/2}^{l/2}\exp(ik\delta z)dz\right) \tag{2.74}$$

$$I_\perp^i = -2iE_0\omega\varepsilon_0 a(M^2-1)\left(\int_{-l/2}^{l/2}\exp(ik\delta z)dz\right) \tag{2.75}$$

$$I_\perp^s = 2iE_0\omega\varepsilon_0 a\left(\frac{M^2-1}{M^2+1}\right)\left(\int_{-l/2}^{l/2}\exp(ik\delta z)dz\right) \tag{2.76}$$

$$I_\perp^c = -2iE_0\omega\varepsilon_0 a\left(M^2\frac{M^2-1}{M^2+1}\right)\left(\int_{-l/2}^{l/2}\exp(ik\delta z)dz\right) \tag{2.77}$$

Finally, substituting the equations 2.58-2.61 in the equation 2.62 the fringing and internal nanoimpedances for parallel polarization are obtained:

$$Z_\perp^c = i\frac{1}{l\pi\omega\varepsilon_0}\left[\frac{1}{M^2-\delta^2}\left(\frac{2k\delta^2}{xM^2}-1\right)\right] \tag{2.78}$$

$$Z_\perp^s = -i\frac{1}{l\pi\omega\varepsilon_0}\left[\frac{1}{M^2-\delta^2}\left(\frac{2k\delta^2}{x}-M^2\right)\right] \tag{2.79}$$

2.5 Normal Incidence

The process to deduce the equations in this chapter can also be found at (GROSSI; AMBROSIO, 2019).

Examining the equations 2.63, 2.64, 2.78 and 2.79 for specific and common angles of wave incidence allows one to deepen our analysis and get more insights.

For a normally impinging wave, with $\delta = 0$ ($\xi = \pi/2$), the equations mentioned above simplify to

$$Z^c_{//} = -i\frac{2k}{l\pi\omega\varepsilon_0}\frac{1+M^2}{xM^4} = -i\frac{2}{l\pi a\omega\varepsilon_0}\frac{1+\varepsilon_{rel}}{\varepsilon^2_{rel}} \tag{2.80}$$

$$Z^s_{//} = i\frac{2}{l\pi a\omega\varepsilon_0}\frac{1+\varepsilon_{rel}}{\varepsilon_{rel}} \tag{2.81}$$

$$Z^c_{\perp} = -i\frac{1}{l\pi\omega\varepsilon} \tag{2.82}$$

$$Z^c_{\perp} = i\frac{1}{l\pi\omega\varepsilon} \tag{2.83}$$

Paying close attention, the structure of the equations is very similar to the ones mentioned in the beginning of the chapter 2 for the inductors (2.1) and capacitors (2.2). Depending on the values assigned for the relative permittivity (ε_{rel}), the impedance will have a inductive or capacitive characteristic.

In order to make it more clear, consider the parallel polarization case:

For the internal impedance, whenever $\varepsilon_{rel} > -1$ (including the plasmonics with $-1 < \varepsilon_{rel} < 0$ and dielectrics with $\varepsilon > 0$) the cylinder behaves as a capacitor, since the equation 2.83 has a negative value. The variable C (capacitance) from equation 2.2 reads as

$$C^c_{//} = \frac{l\pi a\varepsilon_0}{2}\frac{\varepsilon^2_{rel}}{1+\varepsilon_{rel}}, \qquad \varepsilon_{rel} > -1 \tag{2.84}$$

It is important to notice that for $\varepsilon_{rel} = -1$ it would act as a short circuit, and for $\varepsilon_{rel} = 0$ it acts as an open circuit.

Also for the internal impedance, when $\varepsilon_{rel} < -1$ the cylinder behaves as an inductor and can be compared with equation 2.1. The inductance L that reads as

$$L^c_{//} = -\frac{2}{l\pi a\omega^2\varepsilon_0}\frac{1+\varepsilon_{rel}}{\varepsilon^2_{rel}}, \qquad \varepsilon_{rel} < -1 \tag{2.85}$$

The same can be done for the fringing impedance. If $-1 < \varepsilon_{rel} < 0$ the cylinder behaves as a capacitor with C corresponding to

$$C^s_{//} = -\frac{l\pi a\varepsilon_0}{2}\frac{\varepsilon_{rel}}{1+\varepsilon_{rel}}, \qquad -1 < \varepsilon_{rel} < 0 \tag{2.86}$$

And again for the fringing impedance, the cylinder acts as an inductor for $\varepsilon_{rel} > 0$ and $\varepsilon_{rel} < -1$. The inductance L is given by

$$L^s_{//} = \frac{2}{l\pi a\omega^2\varepsilon_0}\frac{1+\varepsilon_{rel}}{\varepsilon_{rel}}, \qquad \varepsilon_{rel} < -1 or \varepsilon_{rel} > 0 \tag{2.87}$$

Consequently, whenever the cylinder is dielectric ($\varepsilon_{rel} > 0$) a resonance will occur and $Z^c_{//} + Z^s_{//} = 0$ for $\varepsilon = 1$.

Equivalently, one can derive the C and L variables for the perpendicular polarization. For the internal impedance:

$$C_{\perp}^{c} = l\pi\varepsilon, \qquad \varepsilon > 0 \tag{2.88}$$

$$L_{\perp}^{c} = -\frac{1}{l\pi\omega^2\varepsilon}, \qquad \varepsilon < 0 \tag{2.89}$$

Nevertheless, the fringing impedance will always be associated with an inductor, regardless of the permittivity ε of the cylinder:

$$L_{\perp}^{s} = \frac{1}{l\pi\omega^2\varepsilon_0}, \qquad \forall\varepsilon \tag{2.90}$$

Notice that for the perpendicular polarization, $Z_{\perp}^{c} + Z_{\perp}^{s} = 0$ only when $\varepsilon_{rel} = 1$, thus the intensity distribution profile of the wave would not be disturbed. Also the average potential difference here will appear between the hemispheres $(\rho = a, 0 < \phi < \pi, z)$ and $(\rho = a, \pi < \phi < 2\pi, z)$.

The impedances have a dependence on l as a consequence of the derivation of the average potential difference and the total displacement currents. Since the integral $\int_{-l/2}^{l/2} exp(ik\delta z)dz$ is indefinite for $z \to \infty$, for the approach to be valid l must be much bigger than the diameter ($l >> a$).

2.6 Parallel Incidence

The process to deduce the equations in this chapter can also be found at (GROSSI; AMBROSIO, 2019).

The same rationale from last section (2.5) will be applied, but now for a plane wave from $+z$ to $-z$ with its electric field always perpendicular to the surface, i.e. $\delta = 1(\xi = 0)$. Using this, to equations 2.63, 2.64, 2.78 and 2.79 simplify to

$$Z_{//}^{c} = -i\frac{2}{l\pi\omega a\varepsilon_0}\frac{1}{(M^2-1)} = -i\frac{2}{l\pi a\omega\varepsilon_0}\frac{1}{(\varepsilon_{rel}-1)} \tag{2.91}$$

$$Z_{//}^{s} = i\frac{2}{l\pi a\omega\varepsilon_0}\frac{M^2}{(M^2-1)} = -\varepsilon_{rel}Z_{//}^{c} \tag{2.92}$$

$$Z_{\perp}^{c} = i\frac{1}{l\pi\omega\varepsilon_0}\left[\frac{1}{M^2-1}\left(\frac{2}{aM^2}-1\right)\right] \approx i\frac{1}{l\pi\omega a\varepsilon_0}\left[\frac{1}{\varepsilon_{rel}(\varepsilon_{rel}-1)}\right] \tag{2.93}$$

$$Z_{\perp}^{s} = -i\frac{1}{l\pi\omega\varepsilon_0}\left[\frac{M^2}{M^2-1}\left(\frac{2}{aM^2}-1\right)\right] \tag{2.94}$$

As expected, the equations above can also be compared with equations 2.1 and 2.2. Assigning values to ε_{rel} for the parallel case, one get the following terms for capacitance and inductance

$$C_{//}^{c} = \frac{l\pi a\varepsilon_0}{2}(\varepsilon_{rel}-1), \qquad \varepsilon_{rel} > 1 \tag{2.95}$$

$$L_{//}^{c} = -2\frac{1}{l\pi\omega^2 a\varepsilon_0(\varepsilon_{rel}-1)}, \qquad \varepsilon_{rel} < 1 \tag{2.96}$$

$$C^s_{//} = -\frac{l\pi a\varepsilon_0}{2}\frac{(\varepsilon_{rel}-1)}{\varepsilon_{rel}}, \qquad 0 < \varepsilon_{rel} < 1 \tag{2.97}$$

$$L^s_{//} = \frac{2}{l\pi a\omega^2\varepsilon_0}\frac{\varepsilon_{rel}}{(\varepsilon_{rel}-1)}, \qquad \varepsilon_{rel} < 0 or \varepsilon_{rel} > 1 \tag{2.98}$$

The equations show that for $\varepsilon_{rel} \to 1$, $Z^c_{//}$ and $Z^s_{//}$ tend to behave as an open-circuit. For $\varepsilon_{rel} = 0$, $Z^c_{//} \to \infty$ and $Z^s_{//} = 0$ (with no current flowing through the circuit). This means that for the wave there is a short-circuit associated with the zero fringing impedance, forcing the current to flow only through the short-circuit.

Now, for the perpendicular polarization

$$C^c_{\perp} = -\frac{l\pi a\varepsilon}{2}(\varepsilon_{rel}-1), \qquad 0 < \varepsilon_{rel} < 1 \tag{2.99}$$

$$L^c_{\perp} = 2\frac{1}{l\pi\omega^2 a\varepsilon(\varepsilon_{rel}-1)}, \qquad \varepsilon > 1 or \varepsilon_{rel} < 0 \tag{2.100}$$

$$C^s_{\perp} = \frac{l\pi a\varepsilon_0}{2}(\varepsilon_{rel}-1), \qquad \varepsilon_{rel} > 1 \tag{2.101}$$

$$L^s_{\perp} = -2\frac{1}{l\pi\omega^2 a\varepsilon_0(\varepsilon_{rel}-1)}, \qquad \varepsilon_{rel} < 1 \tag{2.102}$$

The same conclusion for $\varepsilon_{rel} \to 1$ can be drawn from the equations above: $Z^c_{//}$ and $Z^s_{//}$ tend to behave as an open-circuit. But for $\varepsilon_{rel} = 0$, the current flows through $Z^s_{//} \neq 0$.

3 ANALYTICAL ANALYSIS AND FIELD VISUALIZATION

3.1 Analytical Analysis

After describing the closed-form solutions for the internal and fringing impedances, and investigating closer the $\delta = 1$ and $\delta = 0$ cases, it is important to analyze how each function behaves analytically to get more insights. Values will be used to evaluate specific scenarios.

First, the average potential difference for parallel and perpendicular polarizations will be analyzed. As performed in (GROSSI; AMBROSIO, 2019), in Figure 2, $\langle V \rangle_{//}$ and $\langle V \rangle_{\perp}$ have been normalized by the factor $\frac{E_0}{l} \int_{-l/2}^{l/2} exp(ik\delta z)dz$ and evaluated for four different wave incidence angles varying ε_{rel} from -1.5 to $+1.5$. It was set $ka = 0.001$, $a = 50$ nm (implying $\omega = 6 \times 10^{12}$ rad/s). The normalization is necessary to disconsider the effects of the finite length of the cylinder and, consequently, of the fringing fields, and also the field strength, so one can better analyze the results.

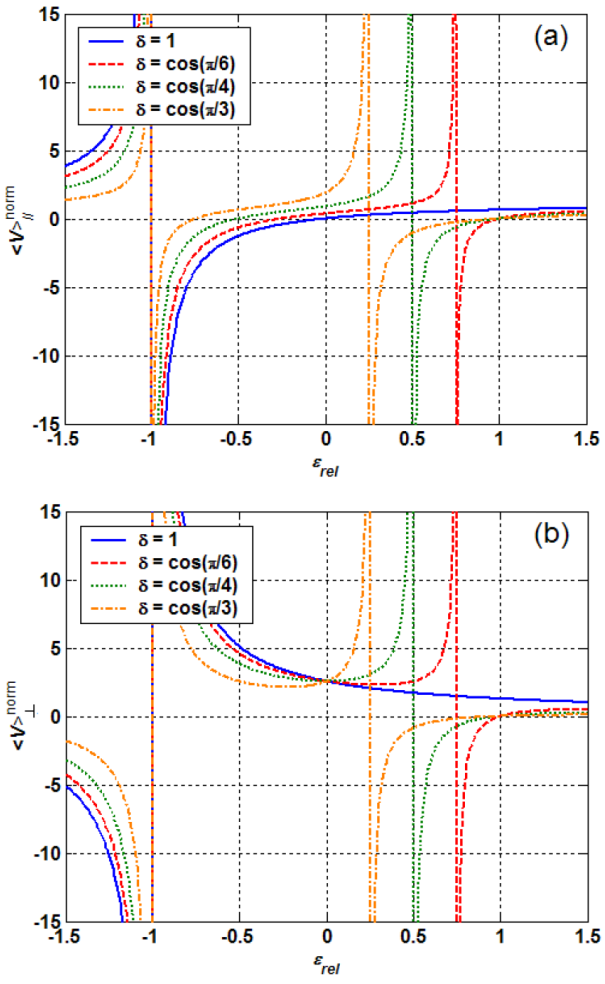

Figure 2: Normalized average potential difference for parallel (a) and perpendicular (b) polarizations as a function of the relative permittivity for different incident angles

For the parallel polarization there are points where $\langle V \rangle_{//} = 0$, them being at $\varepsilon_{rel} = 0$, $\varepsilon_{rel} = -0.5$, $\varepsilon_{rel} = -0.71$ and $\varepsilon_{rel} = -0.87$ for $\xi = 0$, $\xi = \pi/6$, $\xi = \pi/4$ and $\xi = \pi/3$ respectively. This can be deduced inspecting equation 2.43. For passive materials

$$\langle V \rangle_{//} = 0 \quad \rightarrow \quad M = -i\sqrt{1-\delta^2} \tag{3.1}$$

Doing the same for the perpendicular polarization:

$$\langle V \rangle_{\perp} = 0 \quad \rightarrow \quad M = \delta\sqrt{2/a} \tag{3.2}$$

Thus the zero potential is only possible when $\delta \rightarrow 0$ and $2/a >> 1$.

It can also be seen that there are singularities for the potentials, at the points given by $M^2 = \delta^2$ (GROSSI; AMBROSIO, 2019). This can be deduced from equations 2.43 and 2.65. These singularities can be eliminated including losses, that can be done by introducing resistors to the model. This will not be done in the study.

Now, the analysis will be done for the nanoimpedances. The functions in analysis will be from equations 2.63, 2.64 for the parallel polarization and from 2.78, 2.79 for the perpendicular case. It was set $ka = 0.001$, $a = 10$ nm, $l/a = 100$ (configuring an infinite cylinder) and again the plots will vary for ε_{rel} ranging from $-1,5$ to $+1,5$ (divided for the positive and negative values).

When the nanoimpedance assume a negative value, it should be understood as a nanocapacitor. And when positive, should be understood as a nanoinductor. From the equations mentioned in the last paragraph, one can deduce (this can also be found at (GROSSI; AMBROSIO, 2019)):

$$C^c_{//} = \frac{1}{\omega |Z|^c_{//}} = \left[\frac{2}{l\pi\varepsilon_0} \frac{1+\varepsilon_{rel}-\delta^2}{a\varepsilon_{rel}(\varepsilon_{rel}-\delta^2)} \right]^{-1}, \qquad |Z|^c_{//} < 0 \tag{3.3}$$

$$L^c_{//} = \frac{|Z|^c_{//}}{\omega} = \frac{2}{l\pi\omega^2\varepsilon_0} \frac{1+M^2-\delta^2}{aM^2(M^2-\delta^2)}, \qquad |Z|^c_{//} > 0 \tag{3.4}$$

$$C^c_{\perp} = \frac{1}{\omega |Z|^c_{\perp}} = \left\{ \frac{1}{l\pi\varepsilon_0} \left[\frac{1}{(M^2-\delta^2)} \left(\frac{2k\delta^2}{xM^2} - 1 \right) \right] \right\}^{-1}, \qquad |Z|^c_{\perp} < 0 \tag{3.5}$$

$$L^c_{\perp} = \frac{|Z|^c_{\perp}}{\omega} = \frac{1}{l\pi\omega^2\varepsilon_0} \left[\frac{1}{(M^2-\delta^2)} \left(\frac{2k\delta^2}{xM^2} - 1 \right) \right], \qquad |Z|^c_{\perp} < 0 \tag{3.6}$$

Figures 2 and 3 refer to the parallel polarization for the fringing and internal impedances, respectively. Figures 4 and 5 refer to the perpendicular polarization for the fringing and internal impedances, respectively.

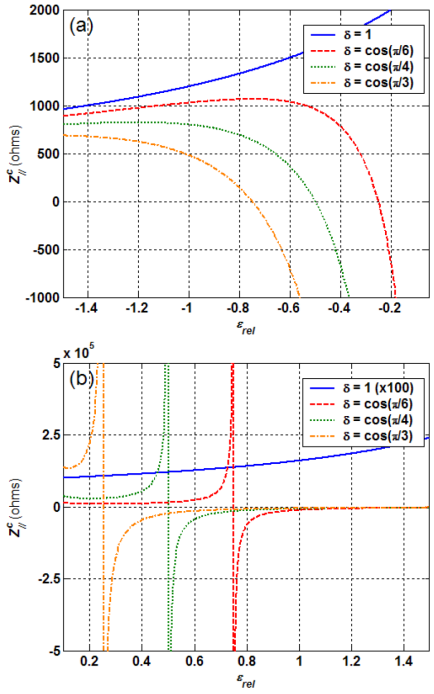

Figure 3: Internal nanoimpedance as a function of ε_{rel} for a parallel polarization; the slope for $\delta = 1$ is multiplied by 100

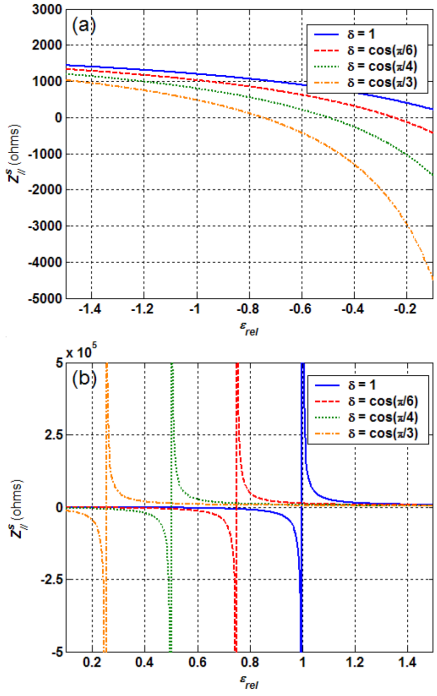

Figure 4: Fringing nanoimpedance as a function of ε_{rel} for a parallel polarization

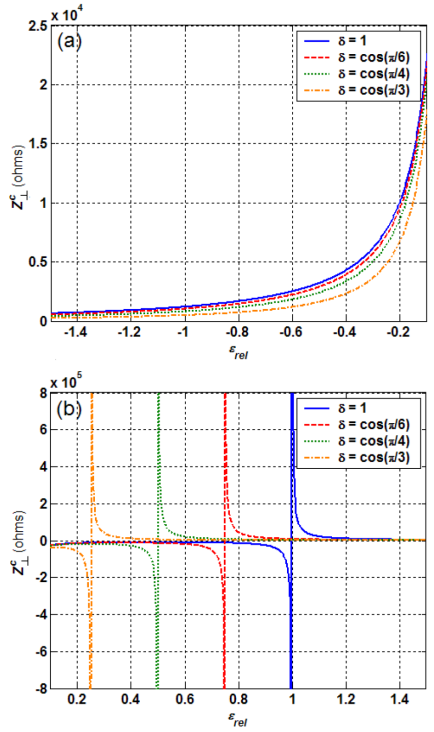

Figure 5: Internal nanoimpedance as a function of ε_{rel} for a perpendicular polarization

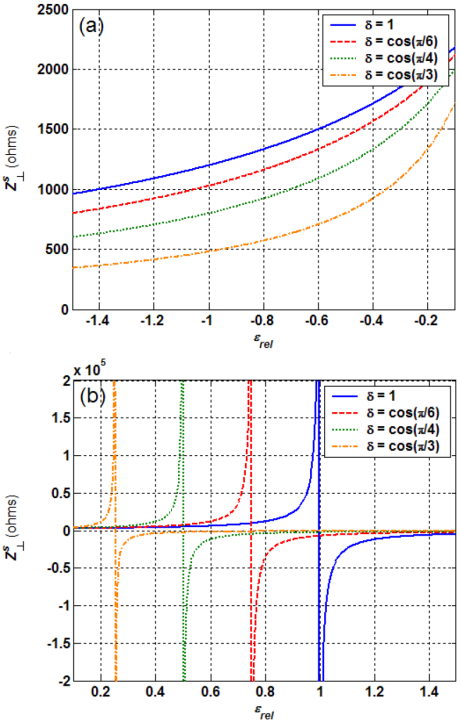

Figure 6: Fringing nanoimpedance as a function of ε_{rel} for a perpendicular polarization

In Figure 3, for $\delta = cos(\pi/4)$ the impedance is characterized by an inductor for ε_{rel} from $-\infty$ to -0.5 and also from 0.25 to $+\infty$. For ε_{rel} between -0.5 and the singularity at 0.25 it acts as a capacitor for example. Also, for $\varepsilon_{rel} = -0.4$, if $\delta = cos(\pi/4)$ one has a capacitive behavior (negatively valued impedance). For the same ε_{rel}, using $\delta = cos(\pi/6)$ the behavior is of an inductor (positive impedance). Thus, varying δ or ε_{rel} one can achieve different behavior, as previously predicted.

This analysis can be done for all the graphs.

3.2 Electric Field Visualization

Finally, to get some more physical insights of the problem, using the commercial software Mathematica 12.0, two situations are analyzed and the incident and scattered electric fields are spatially plotted. Besides seeing how the electric field scatters, this simulation will be used as a parameter to confirm if a future simulation done with the software COMSOL Multiphysics is correctly solving the problem. It will be published in (GROSSI; AMBROSIO, 2019).

The logical path to make this simulation is to use the equations for the fields derived previously in this work. However, besides being an interesting conceptual problem, calculating the beam shape coefficients (BSCs) is a fairly complex task. In order to avoid it, the equations described in (BOHREN; HUFFMAN, 1998) in the section 8.4 are adapted to fit this purpose. Basically, the only equations needed are the expansion of the plane-wave and its respective scattered fields. In the book, the deductions are done using a vectorial approach, instead of the scalar method used previously (the Bromwich method).

3.2.1 Parallel Polarization

The equations used are here shortly introduced. Details can be found at (BOHREN; HUFFMAN, 1998).

One may observe that the equations 2.30 and 2.34 can be reduced to the equations 3.8 and 3.9 bellow for the case of a plane-wave. It is important to notice that the time harmonic factor used throughout this work is $exp(+i\omega t)$, but in the formulation from (BOHREN; HUFFMAN, 1998), $exp(-i\omega t)$ is used. Thus, it implies the inversion of the Hankel function from $H_m^{(2)}$ to $H_m^{(1)}$. Also, in this formulation, there is no dependence on the cylinder length.

The wave considered for this formulation is the same that was previously used in chapter 2, but with the inversion of the time harmonic factor. Thus, the incident electric field is described by the equation 2.3 with a negative exponential signal instead of the positive.

$$\mathbf{E}_i^{//} = E_0(\sin\xi\hat{\mathbf{e}}_z - \cos\xi\hat{\mathbf{e}}_x) \times \exp[-ik(\rho\sin\xi\cos\phi + z\cos\xi)] \tag{3.7}$$

It can be expanded in cylindrical vectorial harmonic functions. The scattered field follows a similar process. Based on the section 8.4 from (BOHREN; HUFFMAN, 1998), one can write for the parallel polarization:

$$E_i = \sum_{n=-\infty}^{\infty} \frac{(-i)^n E_0}{k\sin\xi} N_n^{(1)} \tag{3.8}$$

$$E_s = -\sum_{n=-\infty}^{\infty} \frac{(-i)^n E_0}{k\sin\xi}\left[ia_n M_n^{(3)} + b_n N_n^{(3)}\right] \tag{3.9}$$

In equations above, and for the perpendicular case that will be presented in next section, one has:

$$M_n^{(1)} = \sqrt{k^2-(-k\cos\xi)^2}\left(in\frac{J_n(k\rho\sin\xi)}{k\rho\sin\xi}\hat{\rho} - J_n'(k\rho\sin\xi)\hat{\phi}\right)\exp[i(n\phi - kz\cos\xi)] \tag{3.10}$$

$$M_n^{(3)} = \sqrt{k^2-(-k\cos\xi)^2}\left(in\frac{H_n^{(1)}(k\rho\sin\xi)}{k\rho\sin\xi}\hat{\rho} - H_n'^{(1)}(k\rho\sin\xi)\hat{\phi}\right)\exp[i(n\phi - kz\cos\xi)] \tag{3.11}$$

$$\begin{aligned} N_n^{(1)} = \frac{\sqrt{k^2-(-k\cos\xi)^2}}{k}\Bigg(&- ik\cos\xi J_n'(k\rho\sin\xi)\hat{\rho} + nk\cos\xi\frac{J_n(k\rho\sin\xi)}{k\rho\sin\xi}\hat{\phi} \\ &+\sqrt{k^2-(-k\cos\xi)^2}J_n(k\rho\sin\xi)\hat{z}\Bigg)\exp[i(n\phi - kz\cos\xi)] \end{aligned} \tag{3.12}$$

$$\begin{aligned} N_n^{(3)} = \frac{\sqrt{k^2-(-k\cos\xi)^2}}{k}\Bigg(&- ik\cos\xi H_n'^{(1)}(k\rho\sin\xi)\hat{\rho} + nk\cos\xi\frac{H_n^{(1)}(k\rho\sin\xi)}{k\rho\sin\xi}\hat{\phi} \\ &+\sqrt{k^2-(-k\cos\xi)^2}H_n^{(1)}(k\rho\sin\xi)\hat{z}\Bigg)\exp[i(n\phi - kz\cos\xi)], \end{aligned} \tag{3.13}$$

being m the relative refractive index, a_n and b_n given by:

$$a_n = \frac{C_n V_n - B_n D_n}{W_n V_n - iD_n^2} \tag{3.14}$$

$$b_n = \frac{W_n B_n + iD_n C_n}{W_n V_n - iD_n^2}, \tag{3.15}$$

where

$$\begin{aligned} B_n = ka\sin\xi\Bigg[&m^2 ka\sin\xi J_n'\left(ka\sqrt{m^2-\cos^2\xi}\right)J_n(ka\sin\xi) \\ &-ka\sqrt{m^2-\cos^2\xi}J_n\left(ka\sqrt{m^2-\cos^2\xi}\right)J_n'(ka\sin\xi)\Bigg] \end{aligned} \tag{3.16}$$

$$\begin{aligned} C_n = n(\cos\xi)ka\sqrt{m^2-\cos^2\xi}J_n\left(ka\sqrt{m^2-\cos^2\xi}\right)J_n(ka\sin\xi) \\ \left(\frac{(ka\sin\xi)^2}{k^2a^2(m^2-\cos^2\xi)} - 1\right) \end{aligned} \tag{3.17}$$

$$\begin{aligned} D_n = n(\cos\xi)ka\sqrt{m^2-\cos^2\xi}J_n\left(ka\sqrt{m^2-\cos^2\xi}\right)H_n^{(1)}(ka\sin\xi) \\ \left(\frac{(ka\sin\xi)^2}{k^2a^2(m^2-\cos^2\xi)} - 1\right) \end{aligned} \tag{3.18}$$

$$V_n = ka\sin\xi\Big[m^2 ka\sin\xi J_n'\Big(ka\sqrt{m^2-\cos^2\xi}\Big)H_n^{(1)}(ka\sin\xi) \\ -ka\sqrt{m^2-\cos^2\xi}J_n\Big(ka\sqrt{m^2-\cos^2\xi}\Big)H_n'^{(1)}(ka\sin\xi)\Big] \tag{3.19}$$

$$W_n = ika\sin\xi\Big[ka\sqrt{m^2-\cos^2\xi}J_n\big(ka\sqrt{m^2-\cos^2\xi}\big)H_n'^{(1)}(ka\sin\xi) \\ -ka\sin\xi J_n'\Big(ka\sqrt{m^2-\cos^2\xi}\Big)H_n^{(1)}(ka\sin\xi)\Big] \tag{3.20}$$

In 3.14 to 3.20, there is the assumption that the cylinder does not have magnetic properties, i.e., its permeability is $\mu = \mu_0$. Also, it is important to notice that the equations are for the incident and scattered fields that are valid only for $r \geq a$ (the region outside of the cylinder).

Now, since the ρ component is of interest, one may deduce:

$$E_\rho^i = \sum_{n=-Nmax}^{Nmax}\left(\frac{(-i)^n}{k\sin(\xi i)}N_n^{(1)}\right) \tag{3.21}$$

$$E_\rho^s = -\sum_{n=-Nmax}^{Nmax}\left(\frac{(-i)^n}{k\sin(\xi i)}(ia_n M_n^{(3)} + b_n N_n^{(3)})\right) \tag{3.22}$$

The evaluation of the field component is done for $n = -10$ to $n = 10$, which is sufficient. This number has been evaluated using the following equation, used for truncation of terms for the case of a sphere ():

$$Nmax = kr + 4(kr)^{1/3} + 1 \tag{3.23}$$

where r is space where the equation is evaluated and k is the wave number. It is accurate if 0.02 μm $< r < 8$ μm. Other values were tested to assure the validity for the cylinder case.

The equations above can be written in Mathematica and evaluated for a particular situation.

The cylinder has to have its radius much smaller than the wavelength of the incident wave. A good value is $a = \lambda/20$. Thus, setting $\lambda = 600$ nm (in the optical spectrum), makes $a = 30$ nm. The expressions assume an infinite length, so no value must be defined. The cylinder is spatially oriented as described in 1. $\xi = \pi/4$.

For the material, there are two different ones. The first is a dielectric with the relative refractive index $n = 1.2$. And the second, in order to simulate a plasmonic, $n = 1.2i$. Both non-magnetic ($\mu = \mu_0$).

To clarify, n, the relative refractive index, is given by

$$n^2 = \varepsilon\mu \tag{3.24}$$

, which means that, since the relative permeability is 1, the permitivitty is $\varepsilon = -(1.2)^2$.

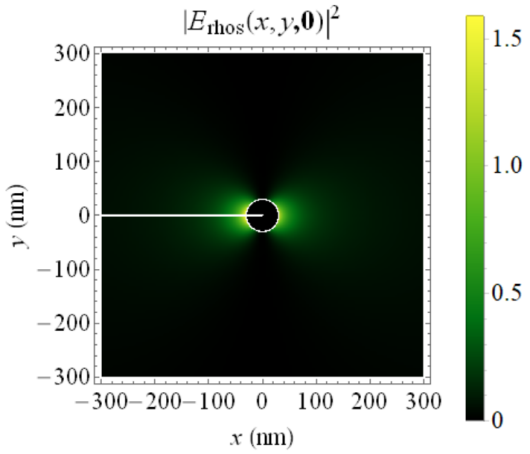

Figure 7: Incident and scattered electric field components for a parallel polarized incident plane wave impinging over a nanocylinder with $n = 1.2i$; xy view

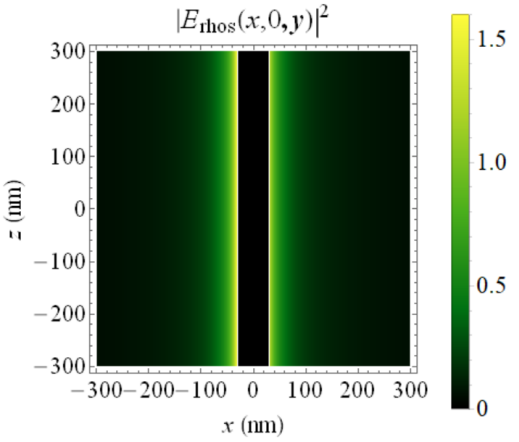

Figure 8: Incident and scattered electric field components for a parallel polarized incident plane wave impinging over a nanocylinder with $n = 1.2i$; xz view

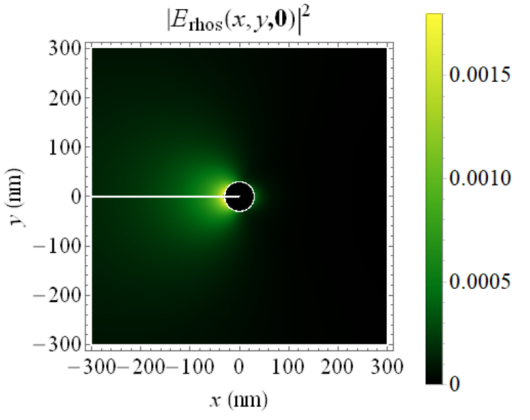

Figure 9: Incident and scattered electric field components for a parallel polarized incident plane wave impinging over a nanocylinder with $n = 1.2$; xy view

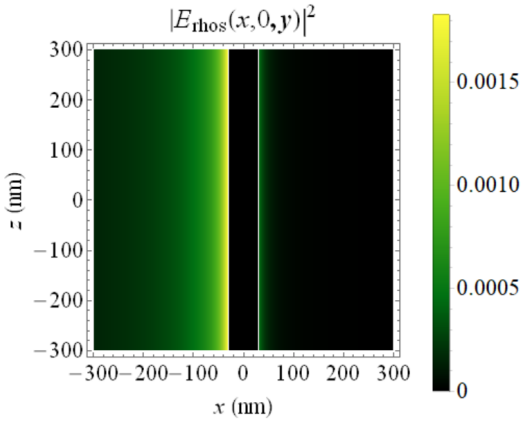

Figure 10: Incident and scattered electric field components for a parallel polarized incident plane wave impinging over a nanocylinder with $n = 1.2$; xz view

The results can be seen clearly in the Figures 7 to 10. As expected, the incident and scattered electric fields are stronger near the nanocylinder, since the higher order terms have less impact.

Another effect to consider is the electric dipole between two hemispheres of the cylinder surface. This can be seen analyzing mainly the Figures 7 and 9. The plasmonic material generated a more symmetrical dipole, but for the dielectric it can still be seen. The importance of such behavior is that to calculate the nanoimpedance, as seen previously, it is necessary to calculate the average potential difference the hemispheres. Analyzing equation 2.62, the bigger the average potential difference the greater is the impedance value.

3.2.2 Perpendicular Polarization

The perpendicular case follows the same procedure done for the parallel case.

The incident electric field equations has also the inverted exponential signal:

$$\mathbf{E}_i^{\perp} = E_0 \hat{\mathbf{e}}_y exp[-ik(\rho sin\xi cos\phi + zcos\xi)] \tag{3.25}$$

Instead of 3.21 and 3.22, one has

$$E_i = -i \sum_{n=-\infty}^{\infty} \frac{(-i)^n E_0}{k \sin\xi} M_n^{(1)} \tag{3.26}$$

$$E_s = \sum_{n=-\infty}^{\infty} \frac{(-i)^n E_0}{k \sin\xi} \left[i c_n M_n^{(3)} + d_n N_n^{(3)} \right], \tag{3.27}$$

where c_n and d_n are

$$c_n = -\frac{A_n V_n - i C_n D_n}{W_n V_n - i D_n^2} \tag{3.28}$$

$$d_n = -i \frac{C_n W_n + A_n D_n}{W_n V_n - i D_n^2}, \tag{3.29}$$

with the same B_n, C_n, D_n, V_n and W_n and now A_n where

$$A_n = ika\sin\xi\Big[-ka\sqrt{m^2-\cos^2\xi}J_n\big(ka\sqrt{m^2-\cos^2\xi}\big)J_n'(ka\sin\xi) \\ +ka\sin\xi J_n'\Big(ka\sqrt{m^2-\cos^2\xi}\Big)J_n(ka\sin\xi)\Big] \tag{3.30}$$

The situations for the simulations are exactly the same as the previous section 3.2.1, except that now the impinging plane-wave is perpendicularly polarized.

The results in the Figures 11 to 14 are similar to those found before. One important insight is that the dipole is no longer found in the x-axis direction, but on the y-axis'.

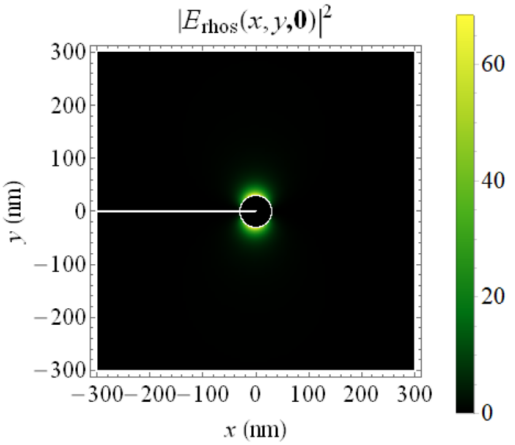

Figure 11: Incident and scattered electric field components for a perpendicularly polarized incident plane wave impinging over a nanocylinder with $n = 1.2i$; xy view

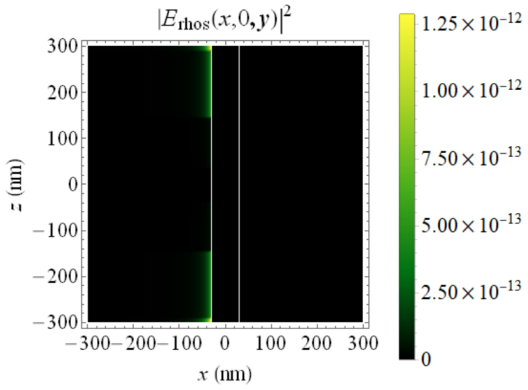

Figure 12: Incident and scattered electric field components for a perpendicularly polarized incident plane wave impinging over a nanocylinder with $n = 1.2i$; xz view

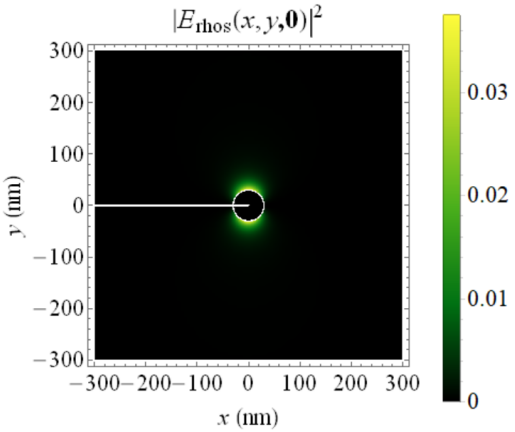

Figure 13: Incident and scattered electric field components for a perpendicularly polarized incident plane wave impinging over a nanocylinder with $n = 1.2$; xy view

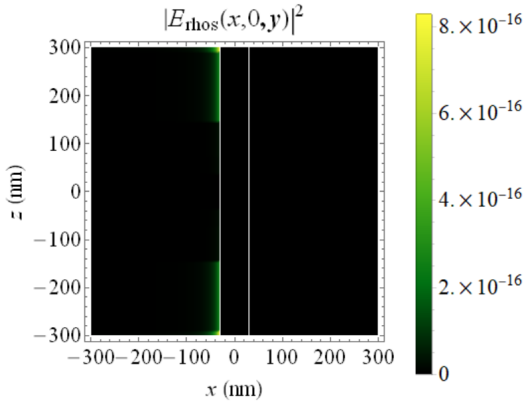

Figure 14: Incident and scattered electric field components for a perpendicularly polarized incident plane wave impinging over a nanocylinder with $n = 1.2$; xz view

These plots will be used for future reference in other articles.

4 CONCLUSION

The expressions for the nanoimpedances were analytically deduced using the GLMT theory. The dependence on the wave's incidence angle and the material's electric and magnetic properties were observed. Also, for specific conditions, the capacitive and inductive behavior were mathematically analyzed.

Later, through a analytical point of view, the equations were investigated and revealed points of resonances and, for a specific situation, the regions in which the cylinder acted as capacitor or inductor. And finally, the electric field expansions were evaluated bringing insights on how it reacted to the nanocylinder and unveiled the expected generation of a dipole.

This research successfully expanded other articles, and hopefully will be further expanded. There are numerous possibilities for future works. A study can be done regarding the validity of the expressions derived here for bigger incidence angles. Also, new numerical analysis can be done in order to analyze different parameters. Additionally, simulations may be executed using commercial softwares based on finite elements method, such as COMSOL Multiphysics, HFSS, CST and others.

BIBLIOGRAPHY

ALÙ, A.; ENGHETA, N. Optical 'shorting wires'. **Opt. Express**, OSA, v. 15, n. 21, p. 13773–13782, Oct 2007.

____. All optical metamaterial circuit board at the nanoscale. **Physical review letters**, v. 103, p. 143902, 10 2009.

ALÙ, A.; SALANDRINO, A.; ENGHETA, N. Parallel, series, and intermediate interconnections of optical nanocircuit elements. 2. nanocircuit and physical interpretation. **J. Opt. Soc. Am. B**, OSA, v. 24, n. 12, p. 3014–3022, Dec 2007.

AMBROSIO, L. A.; HERNÁNDEZ-FIGUEROA, H. E. Plasmonic and dielectric nano-cylinders: Lumped nano-capacitors and nano-inductors from plane waves with arbitrary orientation and polarization. In: **2013 7th International Congress on Advanced Electromagnetic Materials in Microwaves and Optics**. [S.l.: s.n.], 2013. p. 280–282.

BOHREN, C.; HUFFMAN, D. R. **Absorption and Scattering of Light by Small Particles**. [S.l.]: Wiley Science Paperback Series, 1998.

CAI, W.; SHALAEV, V.; PAUL, D. K. Optical metamaterials: Fundamentals and applications. **Physics Today - PHYS TODAY**, v. 63, 09 2010.

CALLEGARO, L. **Electrical impedance: principles, measurement, and applications**. [S.l.]: CRC Press, Taylor Francis Group, 2016.

ENGHETA, N. Circuits with light at nanoscales: Optical nanocircuits inspired by metamaterials. **Science**, American Association for the Advancement of Science, v. 317, n. 5845, p. 1698–1702, 2007. ISSN 0036-8075.

____. Optical metatronics. In: **CLEO: 2011 - Laser Science to Photonic Applications**. [S.l.: s.n.], 2011. p. 1–2. ISSN 2160-8989.

ENGHETA, N.; SALANDRINO, A.; ALÙ, A. Circuit elements at optical frequencies: Nanoinductors, nanocapacitors, and nanoresistors. **Phys. Rev. Lett.**, American Physical Society, v. 95, p. 095504, Aug 2005.

ESTAKHRI, N. M.; EDWARDS, B.; ENGHETA, N. Inverse-designed metastructures that solve equations. **Science**, American Association for the Advancement of Science, v. 363, n. 6433, p. 1333–1338, 2019. ISSN 0036-8075.

GERSHENFELD, N. **The Physics of Information Technology**. [S.l.]: Cambridge University Press, 2000. (Cambridge Series on Informatio). ISBN 9780521580441.

GOUESBET, G. Interaction between an infinite cylinder and an arbitrary-shaped beam. **Appl. Opt.**, OSA, v. 36, n. 18, p. 4292–4304, Jun 1997.

____. Generalized lorenz–mie theories, the third decade: A perspective. **Journal of Quantitative Spectroscopy and Radiative Transfer**, v. 110, n. 14, p. 1223 – 1238, 2009. ISSN 0022-4073. XI Conference on Electromagnetic and Light Scattering by Non-Spherical Particles: 2008.

GOUESBET, G.; GRÉHAN, G. **Generalized Lorenz-Mie Theories**. [S.l.]: Springer International Publishing. ISBN 9783319468723.

____. Interaction between shaped beams and an infinite cylinder, including a discussion of gaussian beams. **Particle & Particle Systems Characterization**, v. 11, n. 4, p. 299–308, 1994.

GROSSI, M. C.; AMBROSIO, L. A. Optical camouflage and transparency with metamaterials. **24 Simpósio Internacional de Iniciação Científica da USP**, 2016.

____. Nano-impedances for infinite cylinders: The plane wave case with arbitrary orientation and polarization. **To be published**, 2019.

KSHETRIMAYUM, R. A brief intro to metamaterials. **Potentials, IEEE**, v. 23, p. 44 – 46, 02 2005.

SALANDRINO, A.; ALÙ, A.; ENGHETA, N. Parallel, series, and intermediate interconnections of optical nanocircuit elements. 1. analytical solution. **J. Opt. Soc. Am. B**, OSA, v. 24, n. 12, p. 3007–3013, Dec 2007.

SILVEIRINHA, M. G. et al. Nanoinsulators and nanoconnectors for optical nanocircuits. **Journal of Applied Physics**, v. 103, n. 6, p. 064305, 2008.

WEST, P. et al. Searching for better plasmonic materials. **Laser & Photonics Reviews**, v. 4, n. 6, p. 795–808, 2010.